Dalton Transactions

Accepted Manuscript

This is an *Accepted Manuscript*, which has been through the RSC Publishing peer review process and has been accepted for publication.

Accepted Manuscripts are published online shortly after acceptance, which is prior to technical editing, formatting and proof reading. This free service from RSC Publishing allows authors to make their results available to the community, in citable form, before publication of the edited article. This *Accepted Manuscript* will be replaced by the edited and formatted *Advance Article* as soon as this is available.

To cite this manuscript please use its permanent Digital Object Identifier (DOI®), which is identical for all formats of publication.

More information about *Accepted Manuscripts* can be found in the **Information for Authors**.

Please note that technical editing may introduce minor changes to the text and/or graphics contained in the manuscript submitted by the author(s) which may alter content, and that the standard **Terms & Conditions** and the **ethical guidelines** that apply to the journal are still applicable. In no event shall the RSC be held responsible for any errors or omissions in these *Accepted Manuscript* manuscripts or any consequences arising from the use of any information contained in them.

Dendritic CdS assembles for removal of organic dye molecules

Zhou Yu, Fengyu Qu*, Xiang Wu*

Key Laboratory for Photonic and Electronic Bandgap Materials, Ministry of Education and College of Chemistry and Chemical Engineering, Harbin Normal University, Harbin 150025, P. R. China

In this paper, novel CdS 3D assemblies are prepared via a facile and effective hydrothermal route using dimethyl sulfoxide as the growth template. Morphologies, microstructures and photocatalytic properties of the as-synthesized products are investigated in detail. It was found that dimethyl sulfoxide played an important role in the formation of CdS assemblies. A possible growth mechanism for CdS assemblies was proposed based on the experimental results. In addition, CdS assemblies exhibit superior photocatalytic activities by the photodegradation of eosin B, Methyl orange (MO) and Rhodamine B (RhB) under visible light irradiation, with a comparison with other CdS nanostructures, P25 and a-Fe_2O_3 powders, demonstrating potential applications in removal of organic dye molecules from waste water.

Author to whom correspondences should be addressed:

E-mail: wuxiang05@gmail.com and qufengyu@hrbnu.edu.cn

1 Introduction

Nowadays, environmental pollution and destruction on a global scale have attracted more and more attention.[1-5] For the sustainable development of human society, to develop both pollution-free technologies for environmental remediation and alternative clean energy supplies is an urgent task.[6] Semiconductor photocatalysis can provide a simple way to induce degradation of organic pollutants by UV/Vis light irradiation.[7-11] It can be expected that novel micro/nanostructures are beneficial to efficient photocatalytic degradation of organic pollutants from waste water.

So far, ZnO, TiO_2 and SnO_2 have been regarded as the efficient photocatalysts due to their high catalytic activities, great stabilities, nontoxicity and low cost, but the wide bandgaps hindered their sufficient utilization of sunlight.[11-19] As an important II-VI semiconductor, CdS is regarded as one of the most attractive visible light-driven photocatalysts due to its relatively narrow band gap of 2.42 eV that corresponds well with the solar spectrum.[20-28] It is well-known that nanomaterials' properties greatly depend on their morphological features. Therefore, a great deal of efforts have been devoted to prepare CdS nanomaterials with the desired size and architecture through various methods. For example, Gao and co-workers synthesized three dimensional CdS nanocrystals using hexamethylenetetramine [$(CH_2)_4N_4$, HMT] as a capping reagent.[29] Yu et al. reported a solvothermal approach to synthesize urchin-like CdS flowers and branched nanowires.[23] In our previous report, we obtained dendrite-like CdS hierarchical nanostructures by a facile and effective hydrothermal route at a mild temperature.[30] Although several preparation methods have been proposed to fabricate

CdS nanomaterials, to develop the synthetic strategies for CdS nanocrystals with various morphologies is still very tremendous challenge.

Herein, we prepared successfully a kind of novel 3D CdS assemblies with unique spatial architecture via a simple one-step hydrothermal route using dimethyl sulfoxide (DMSO) as the growth template. A possible growth mechanism of the as-prepared CdS products was proposed. The photocatalytic performances of the as-obtained CdS products for the photodegradation of organic dyes under visual light irradiation were investigated in detail. The results showed that the as-synthesized 3D CdS assemblies possess superior photodegradation activities toward organic dyes molecules.

2 Experimental

All reagents were of an analytical grade and used without further purification. In a typical procedure, 1 mmol $CdCl_2 \cdot 5H_2O$, 3 mmol thiourea ($CH_4N_2O_4S$) and 0.2 ml DMSO were dissolved into 40 ml deionized water in sequence to form a homogeneous solution with constant stirring. After stirring for 30 min, the suspension was transferred into a Teflon-lined stainless steel autoclave with a capacity of 50 ml. The autoclave was sealed and heated in a program-controlled oven at 160 ^{o}C for 10 h. After the system was cooled naturally to room temperature, the precipitates obtained was washed several times with deionized water and ethanol, and then dried in a vacuum at 60 ^{o}C for 10 h.

The phase and composite of the as-obtained product were characterized by X-ray diffraction (XRD, Rigaku Dmax-rB, Cu Ka radiation, λ= 0.1542 nm 40 KV, 100 mA). The morphology and microstructure of the samples were characterized with scanning

electron microscope (SEM, Hitachi-4800), transmission electron microscope (TEM, JEOL 2010EX) and Raman spectroscopy (HR800). A specific surface area analyzer (NOVA2000E) was used to measure the N_2-sorption isotherm. The Brunaue-Emmett-Teller (BET) formula was further used to calculate the specific surface area. The photocatalytic degradation activities were investigated by monitoring dye decolorization at the maximum absorption wavelength, using a UV/Vis spectrometer (Shimazu UV-2550).

The evaluation of photocatalytic performance of as-synthesized samples for photocatalytic decomposing or removing of eosin B, Methyl Orange (MO) and Rhodamine B (RhB) aqueous solution was performed as follows: 0.05 g CdS assemblies were suspended in 200 ml organic dyes aqueous solution (10 mgL^{-1}). The suspensions were magnetically stirred in the dark for 60 min to ensure an adsorption/desorption equilibrium of organic dyes aqueous solution, and the solution was then exposed to an 800 W xenon lamp at room temperature. At given irradiation intervals, a series of aqueous solution was collected for analysis. The photocatalytic performance of the catalyst was evaluated by monitoring the visible absorbance characteristic of the targeted organic dye molecules using UV/Vis spectroscopy. The changes of organic dyes concentration under Xenon lamp irradiation were calculated as follows:

$$I = C/C_0 \times 100\%$$

Where C_0 and C are the equilibrium concentration of organic dyes before and after irradiation, respectively. Photocatalytic activity derived from the changes of organic

dyes concentration can be represented by the relative ratio C/C_0.

3 Results and Discussion

The morphology and microstructural details of the as-prepared 3D CdS assemblies are investigated by SEM and TEM observation. Fig. 1a presents the overall morphology of the as-synthesized CdS assemblies, clearly observing that the product exhibits 3D assemblies microstructure with the diameter of 4-7 μm. Fig. 1b shows single CdS 3D assemblies consisting of quantities of dendrites. Each of them is composed of a central trunk with the length of 3-4 μm and numerous branches with the average length of 500 nm, which distributed parallelly in the central trunk. Single TEM image of CdS 3D assemblies shown in Fig. 1c also confirmed the observations from SEM. The SAED pattern taken from the trunk tip and branch tip were observed to be exactly the same, and the diffraction spots demonstrate that the entire leaf is a CdS single crystal oriented along [0001] with the three branches along[$10\bar{1}0$], [$1\bar{1}00$], and [$0\bar{1}10$], respectively (see Figure 1d). Figure 1e and f are HRTEM images taken from the areas labeled A and B in Figure 1c. The lattice spacing of 0.39 nm and 0.33 nm correspond to the distance between two {$10\bar{1}0$} crystal planes and [0001] crystal planes.

Fig. 2a shows a representative XRD pattern of the as-prepared product, all diffraction peaks can be indexed to hexagonal wurtzite CdS (JCPDS no. 41-1049). No obvious diffraction peaks from other impurities were observed, suggesting high crystallinity of CdS 3D assemblies. Raman scattering spectroscopy was also performed to further study the structures of CdS product. Fig. 2b displays room

temperature Raman spectrum of CdS microstructures. Two Raman peaks centered at 301 and 602 cm^{-1} are observed. They can be assigned to the first and second order longitudinal optical (LO) phonon modes of CdS, respectively.[31,32] The ratio of 2LO mode intensity to 1LO mode intensity, which reflects exciton-photon coupling, was calculated to be 0.48, the ratio is known to decrease in the particle size of CdS.[33,34] The symmetric and sharp peaks of CdS products suggest that CdS 3D assemblies structures are highly crystalline, which is consistent with the XRD results.

Nitrogen adsorption-desorption measurements were conducted to determine the specific surface area and pore size of the CdS 3D assemblies structures. The nitrogen adsorption-desorption isotherm and the corresponding BJH pore diameter distribution of CdS 3D assemblies are presented in Fig. 3. It reveals that the isotherm of the as-synthesized CdS product is a type IV isotherm with H_3-type hysteresis loops according to IUPAC. Quantitative calculation demonstrates that the as-prepared CdS product possesses a BET surface area of 18.276 m^2/g.

To better understand the formation of CdS 3D assemblies, a series of controlled experiments were conducted by varying experimental parameters. At first, time dependent SEM images of the as-synthesized products were investigated, as shown in Fig. S1. In Fig.S1a, at the early stage of the reaction, irregular small particles with the average size of 200 nm aggregate for 0.5 h. With a prolonged time up to 1 h (Fig. S1b), some sheet-like structures through a "back-to-back" way assemble together to form an original parent structure. From this stage, further growth of each sheet would be overwhelmed during formation process of the final product.

When the reaction time is increased to 3 h, the sheets partially split and changed to dendrite structures (Fig. S1c). After reaction of 5 h, the branch-like structure of the dendrite outspread gradually (see in Fig. S1d). From Fig. S1e, one finds further increasing reaction time to 8 h results in the branches of the dendrites increases larger. The hierarchical structure didn't almost change significantly when reaction time was further increased to 10 h (Fig. S1f), revealing extension of reaction times can just affect the size of the as-prepared products.

Fig. S2 shows the as-synthesized products in the presence of different quantities of DMSO at 160 ^{o}C for 10 h. It can be found that without using DMSO the as-obtained products show a dendritic-like structure with a pronounced trunk and highly ordered branches distributed on both sides of the trunk, as shown in Fig. S2a. It is noteworthy that such dendritic-like structures didn't assemble together, showing that DMSO plays a significant role for the growth of dendritic-like structure assembly. When the addition of a dosage DMSO was 0.1 ml, the samples exhibit a smaller size (Fig. S2b) compared with that with addition of the amount of 0.2 ml (Fig. S2c). Further increasing the dosage of DMSO to 0.3 ml (seen from Fig. S2d), the sizes of branches are irregular.

Based on the above experimental results, a possible growth mechanism of CdS 3D assemblies may be proposed as follows: at the initial stage, the Cd^{2+} and the thiourea might form the complex compound (Cd-thiourea) because of the strong coordinating capacity of thiourea. Then, the Cd-thiourea complex may tend to decompose to release the active Cd^{2+} and S^{2-} gradually with the increase of

temperature.[35] At the same time, the DMSO molecules as the surfactant assembly form an arc-like structure in solution, the methyl groups in the molecules of DMSO would be in the interior because of their hydrophobic property, while the S=O group will be at the exterior. The released S^{2-} ions react with the Cd^{2+} ions which are coordinated on the DMSO templates, resulting in the formation of the growth nuclei. With an increase of reaction time, primary nuclei gradually form to the sheet-like structure. The sheet-like CdS nanostructures grow fast along certain directions due to anisotropic characteristic.[36-38] Fig. 4 showed the growth schematic diagram of CdS assembles.

UV-vis diffuse reflectance spectrum was used to investigate the light absorption property of the as-synthesized CdS 3D assemblies. In Figure 5, CdS 3D assemblies exhibit a steep absorption edge located at 548 nm, indicating the sample possesses visible light absorption band, which endows it potential applications in solar catalysis. In comparison to pure eosin B dye molecules, the absorption edge of CdS 3D assemblies with eosin B exhibit a wide visible light absorption band, which could be attributed to the presence of CdS 3D assemblies as visible-light sensitization, which has a strong and wide absorption band in the visible-light region.

To demonstrate potential applications of the as-synthesized CdS 3D assemblies in waste water treatment, photocatalytic activities of the as-obtained products in the degradation of eosin B, RhB and MO dyes were investigated in detail. Absorption spectra of photodegradation of different dyes under visual light irradiation are shown in Fig 6. Fig 6a shows the UV/Vis adsorption spectra of eosin B solution in the

presence of CdS 3D assemblies under visual light at different time intervals. The main absorption peak of eosin B centered at 517 nm before and after irradiation. When the light was turned on, the main peaks decreased continuously with increased irradiation time, indicating that the eosin B solution was decomposed in the present system. The intensity of the absorbance peaks drops rapidly with the elongation of the exposure time and completely disappears after about 80 min, the efficiency is up to 98.7%. Similar photodegradation experiments were also conducted to other target molecules. Fig. 6b shows the absorption spectra of MO aqueous solution for various irradiation durations. When the illumination time was extended to 180 min, the color of the MO solution vanished. The absorption peak corresponding to MO at 465 nm diminished gradually and the photocatalytic degradation rate of MO was 92%. For further comparison, the photocatalytic degradation rates of RhB with CdS 3D assemblies were shown in Fig. 6c. The absorption peak corresponding to RhB is located at 553 nm, and nearly 98% of RhB molecules were decomposed after 220 min. Fig. 6d illustrates a comparison of the degradation rates of the above three dyes under the same condition. It is found that the degradation ratio of eosin B is better than the other two dyes when the irradiation time reaches 80 min.

To further evaluate the degradation capability to eosin B solution with different photocatalysts, Dendritic-like CdS, commercial CdS powders, P25 and a-Fe_2O_3 powders were chosen for the comparison. Fig 7a-7e correspond to the adsorption spectra of eosin B solution in the presence of CdS 3D assemblies, dendritic-like CdS, commercial CdS powders, a-Fe_2O_3 powders and P25 under visual

light at regular intervals. Fig. 7f reveals the photocatalytic degradation ratio of eosin B using several different photocatalysts under the same condition. After irradiation for 80 min, about 92% of eosin B decomposes in the case of dendritic-like CdS as the catalyst (red curve in Fig. 7f) and about 84% of decolorization for commercial CdS powders (blue curve). Green curve also indicates that the poor photocatalytic performance of 46% in the case of P_{25}. Among various semiconductors, a-Fe_2O_3 is also regarded as one of the most attractive visible light-driven photocatalysts. For comparison, the photocatalytic activities of a-Fe_2O_3 powders under xenon lamp irradiation have also been tested. It is found that a-Fe_2O_3 powders degradation rate is only 17% (pink curve). In the absence of Xenon light illumination on eosin B leads to only degradation 10% of the dye at all (yellow curve in Fig. 7f), indicating that the eosin B degradation needs an electron-transfer mediator under visible light. As for CdS 3D assemblies, the degradation rate is 97% after 80 min illumination (black curve), which is evidently greater than that of above photocatalysts. Hence, the order of the decomposition rate of eosin B aqueous solution in the presence of above catalysts is as follows: CdS 3D assemblies (97%) > dendritic - like CdS (92%) > commercial CdS powders (84%) > P25 (46%) > a-Fe_2O_3 powders (17%) > blank experiment (10%). The superior photocatalytic efficiencies of CdS 3D assemblies may be attributed to unique spatial structures, larger surface area and higher crystallinity of the obtained samples[40,41]. It indicates that such CdS 3D assemblies may have potential application in eliminating organic pollutant in waste water.

It is well-known that the photocatalytic oxidation of organic pollutants obeys

Langmuir–Hinshelwood kinetics[42]. This kind of pseudo-first-order kinetics can be represented as follows:

$$r = -dC/dt = -k'KC/1 + KC \quad \text{Eq. (1)}$$

Where r is the rate of dye mineralization, k is the rate constant, C is the dye concentration, and K is the adsorption coefficient. By integration, Eq. (1) can be arranged into the following:

$$InC/C_0 = -kt \quad \text{Eq. (2)}$$

Where C_0 is the initial concentration of the eosin B solution and k is a rate constant. According to Eq. (2), rate constant k can be given by the slope of fitting curves, when plotting $\ln(C/C_0)$ against. The degradation data with the linear fitting curves are plotted in Fig. 8. The reaction rate constants for CdS 3D assemblies, dendritic-like CdS, commercial CdS powders, P25, a-Fe_2O_3 powders and blank experiment are 0.04562 min^{-1}, 0.03212 min^{-1}, 0.02100 min^{-1}, 0.00775 min^{-1}, 0.00182 min^{-1}, and 0.00125 min^{-1} respectively. The results illustrate that the CdS 3D assemblies possess excellent photocatalytic properties than the other photocatalysts under the visible light irradiation.

4 Conclusions

In summary, novel CdS 3D assemblies were prepared via a facile hydrothermal route using DMSO as the growth template. The possible growth mechanism of CdS 3D assemblies was proposed based on the experimental results. The photocatalytic degradation experiments showed that the CdS 3D assemblies exhibit higher photocatalytic activity compared with dendritic-like CdS, commercial CdS powders,

P25 and a-Fe_2O_3 powders. The improved photocatalyst efficiency of CdS 3D assemblies might possess potential application in industry waste water treatment.

Acknowledgement:

This work was supported by the Foundation for Key Project of Ministry of Education, China (No. 211046), Open Fund of State Key Laboratory for Modification of Chemical Fibers and Polymer Materials, Dong Hua University (No. K1012), Program for New Century Excellent Talents in Heilongjiang Provincial University (1252-NCET-018), the Scientific Research Fund of Heilongjiang Provincial Education Department (12531179) and Program for Scientific and Technological Innovation Team Construction in Universities of Heilongjiang (No. 2011TD010).

References and Notes

1. J. A. Lee, K. C. Krogman, M. Ma, R. M. Hill, P. T. Hammond and G. C. Rutledge, *Adv. Mater.*, 2008, **20**, 1252.

2. J. Z. Yang, J. W. Yu, J. Fan, D. P. Sun,W. H. Tang and X. J. Yang, *J. Hazard. Mater*., 2011, **189**, 377.

3. W. N. Jia, B. X . Jia, X. Wu, F. Y. Qu and H. J. Fan, *Sci. Adv. Mater*., 2013, **5**, 1329.

4. J. Wang, F. Y. Qu and X. Wu, *Mater. Express*, 2013, **3**, 256.

5. J. Wang, F. Y. Qu and X. Wu, *Sci. Adv. Mater*., 2013, **5**, 1052.

6. H. Tong, S. X. Ouyang, Y. P. Bi, N. Umezawa, M. Oshikiri and J. H. Ye, *Adv. Mater.*, 2012, **24**, 229.

7. M. D. Hernandez-Alonso, F. Fresno, S. Suarez, and J. M. Coronado, *Energy Environ. Sci.* 2009, **2**, 1231.

8. B. X. Jia, W. N. Jia, X. Wu and F. Y. Qu, *Sci. Adv. Mater.* 2012, **4**,1127.

9. M. N. Liu, H. X. Wang, C. Yan, and J. Bell, *Mater. Focus*. 2012, **1**, 136.

10. S. Y. Song and H. J. Zhang, *Rev. Adv. Sci. Eng*. 2012, **1**, 165.

11. J. Ma, L. S. Qiang, H. Y. Li and X. B. Tang, *Sci. Adv. Mater*, 2012, **4**,539.

12. X. Chen and S. S Mao, *Chem. Rev*. 2007, **107**, 2891.

13. H. Zhang and Y. F. Zhu, *J. Phys. Chem. C*. 2010, **114**, 5822.

14. F. H. Chu, C. W. Huang, C. L. Hsin, C. W. Wang, S. Y. Yu, P. H. Yeh, and W. W. Wu, *Nanoscale*. 2012, **4**, 1471.

15. Y. K. Lai, L. Sun, Y. C. Chen, H. F. Zhuang, C. J. Lin, and J. W. Chen, *J. Electrochem*. *Soc*. 2006, **153**, 123.

16. Y. T. Han, X. Wu, Y. L. Ma, L. H. Gong, F. Y. Qu and H. J. Fan, *CrystEngComm*, 2011, **13**, 3506 .

17. Q. F. Zhang, T. P. Chou, B. Russo, S. A. Jenekhe and G. Z. Cao, *Angew. Chem. Int. Ed.* 2008, **47**, 2402 .

18. B. X. Jia, W. N. Jia, Y. L. Ma, X. Wu, and F. Y. Qu, *Sci. Adv. Mater*. 2012, **4**, 702 .

19. W. N. Jia, B. X. Jia, X. Wu, and F. Y. Qu, *CrystEngComm*. 2012, **14**, 7759.

20. X. S. Fang, T. Y. Zhai, U. K. Gautam, L. Li, L. M. Wu, Y. Bando and D. Golberg, Prog. Mater. Sci., 2011, **56**, 175.

21. L. F. Hu, J. Yan, M. Y. Liao, H. J. Xiang, X. G. Gong, L. D. Zhang and X. S. Fang, *Adv. Mater*., 2012, **24**, 2305.

22. G. Dukovic, M. G. Merkle, J. H. Nelson, S. M. Hughes and A. P. Alivisatos, *Adv. Mater.*, 2008, **22**, 4036.

23. W. T. Yao, S. H. Yu, S. J. Liu, J. P.Chen, X. M. Liu, F. Q. Li, *J. Phys. Chem. B* 2006, **110**, 11704.

24. Z. A. Peng and X. G. Peng, *J. Am. Chem. Soc*. 2001, **123**, 183.

25. L. Dong, T. Gushtyuk and J. Jiao, *J. Phys. Chem. B*, 2004, **108**, 1617.

26. L. D. Nyamen, V. S. R. R. Pullabhotla, A. A. Nejo, P. T. Ndifon, J. H. Warner and N. Revaprasadu, *Dalton Trans*., 2012, **41**, 829.

27. B. J. S. Johnson, J. H.Wolf and A. S. Zalusky, *Chem. Mater.* 2004, **16**, 2909.

28. Y. Guo, J. Wang, Z. K. Tao, F. F. Dong, K. Wang, X. M. Ma, P. H. Yang, P. P. Hu, Y. T. Xu and L. Yang, *CrystEngComm*, 2012, **14**, 1185.

29. F. Gao, Q. Y. Lu, X. K. Meng and S. Komarneni, *J. Phys. Chem. C*, 2008, **112**, 13359.

30. Z. Yu, X. Wu, J. Wang, W. N. Jia, G. S. Zhu, and F. Y. Qu, *Dalton Trans*., 2013, **42**, 4633.

31. G. Z. Shen and C. J. Lee, *Cryst. Growth. Des.* 2005, **5**, 1085.

32. S. Kar and S. Chaudhuri, *J. Phys. Chem. B*. 2006, **110**, 4542.

34. M. R. Kim and D. J. Jang, *Chem. Commun*., 2008, 5218.

35. L. Zeiri, I. Patla, S. Acharya, Y. Golan and S. Efrima, *J. Phys. Chem. C* , 2007, **111**, 11843.

36. Y. M. Guo, J. F. Wang, L. Yang, J. Zhang, K. Jiang, W. J. Li, L. L. Wang and L. L. Jiang, *CrystEngComm*, 2011, **13**, 5045.

37. M. Darko and D. Miha, *Cryst. Growth. Des*., 2008, **8**, 2182.

38. X. B. He and L. Gao, *J. Phys. Chem. C*, 2009, **113**, 10981.

39. S. R. Aghdaee and V. Soleimanian, *J. Cryst. Growth*, 2012, **341**, 66.

40. H. B. Zeng, W. P. Cai, P. S. Liu, X. X. Xu, H. J. Zhou, C.Klingshirn and H. Kalt, *ACS Nano*, 2008, **2**, 1661.

41. H. B. Zeng, G. T. Duan, Y. Li, S. K. Yang, X. X. Xu and W. P. Cai, *Adv. Funct. Mater*, 2010, **20**, 561.

42. R.K. Wahi, W. W. Yu, Y. P . Liu, M. L. Mejia, J. C. Falkner, W. Nolte and V. L. Colvin, J. Mol. *Catal. A: Chem*, 2005, **242**, 48.

Figure captions

Fig. 1 Morphologies of the as synthesized CdS 3D assemblies. (a-b) SEM images at different magnification. (c) TEM image of a single microstructure; (d) selected-area electron diffraction (SAED) pattern of the assynthesized products. (e) and (f) HRTEM image

Fig. 2 (a) XRD pattern of the as-synthesized products (b) Raman spectrum the as-synthesized products

Fig. 3 Nitrogen adsorption/desorption isotherm and Pore diameter distribution of the as-synthesized samples

Fig. 4 Growth Schematic of the as-synthesized CdS 3D assemblies

Fig. 5 UV-Vis diffuse reflection spectra of the as-synthesized CdS 3D assemblies

Fig. 6 Variations of adsorption spectra of organics dye solution in the presence of the CdS 3D assemblies irradiated by a visible lamp for different time: a. Eosin B b. Methyl orange c. Rhodamine B d. photocatalysis degradation rate of eosin B, Methyl orange and Rhodamine B

Fig. 7 Adsorption spectra of Eosin red solution in the presence: a. CdS 3D assemblies b. dendritic-like CdS c. commercial CdS powders d. P25 e. a-Fe_2O_3 powders f. photocatalytic degradation ratio of eosin B using several different photocatalysts under the same condition.

Fig. 8 The linear fitting of the photocatalytic activity

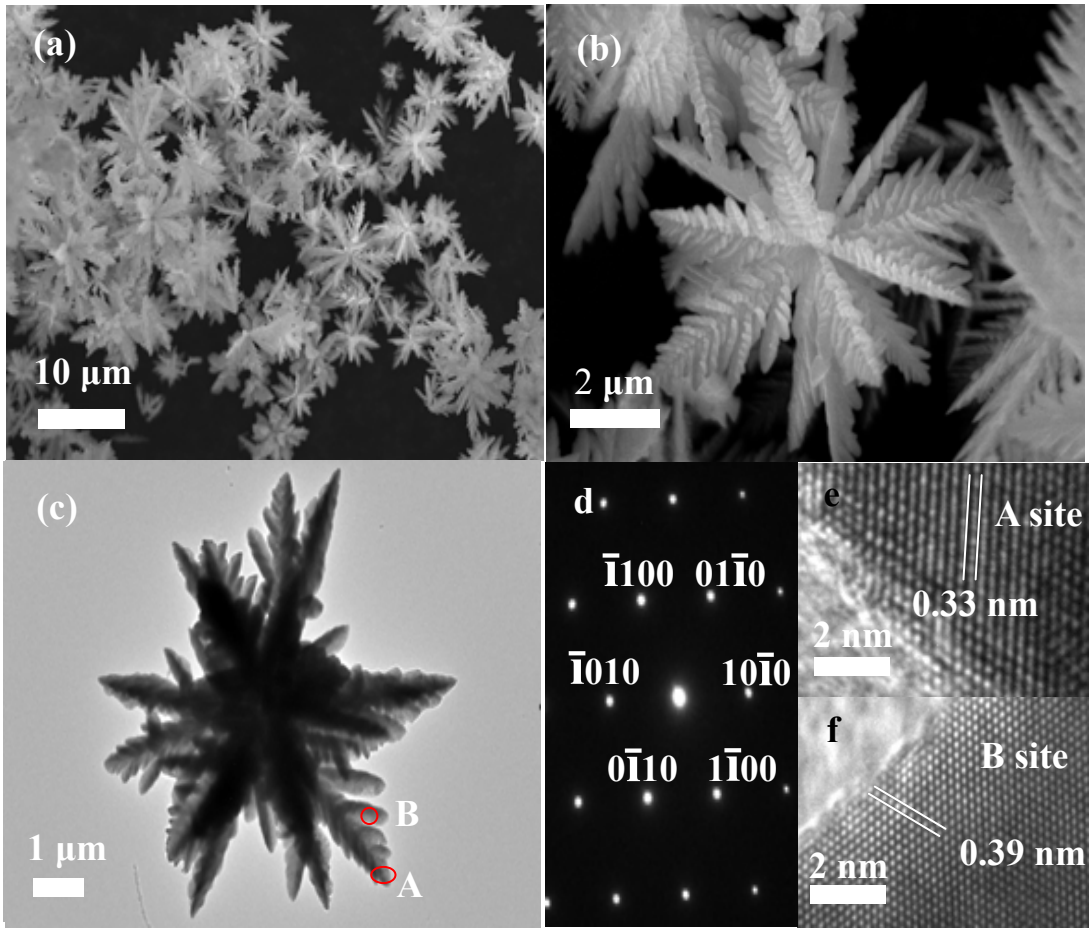

Fig. 1 Zhou Yu et al.

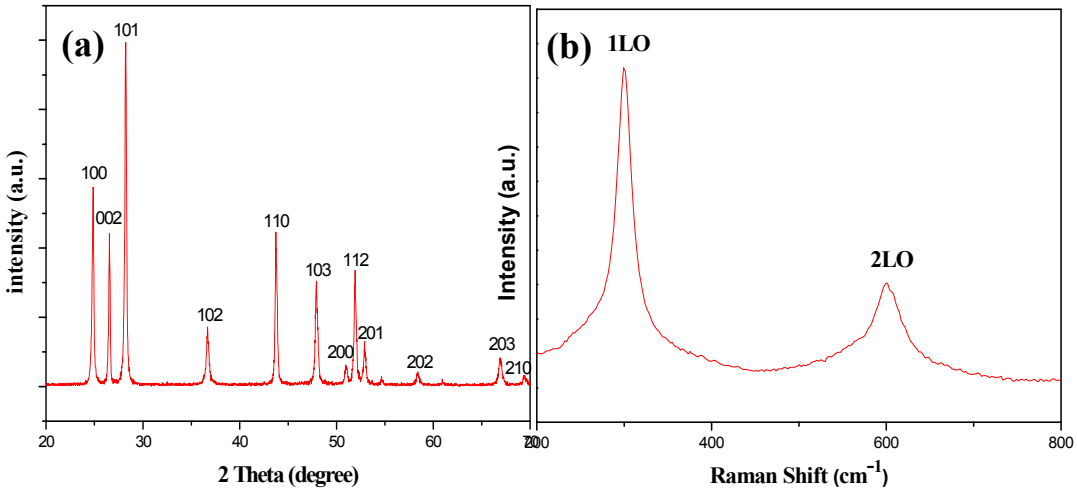

Fig. 2 Zhou Yu et al.

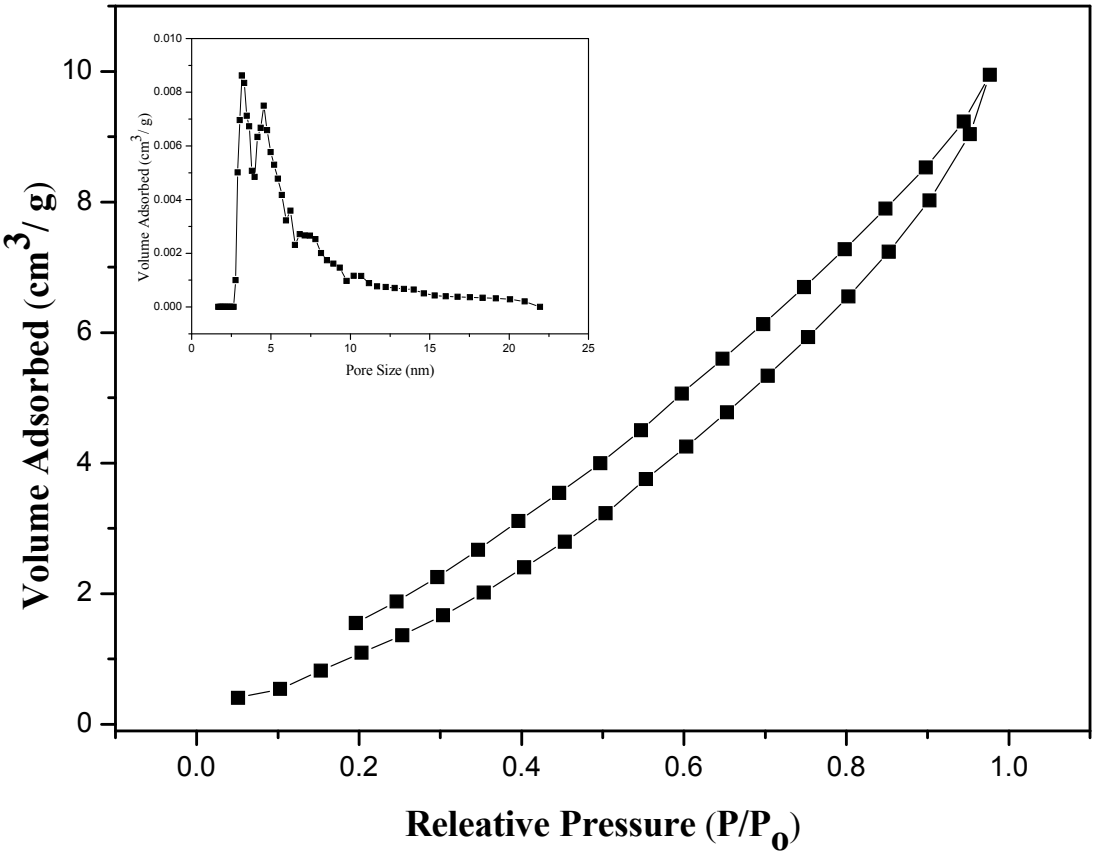

Fig. 3 Zhou Yu et al.

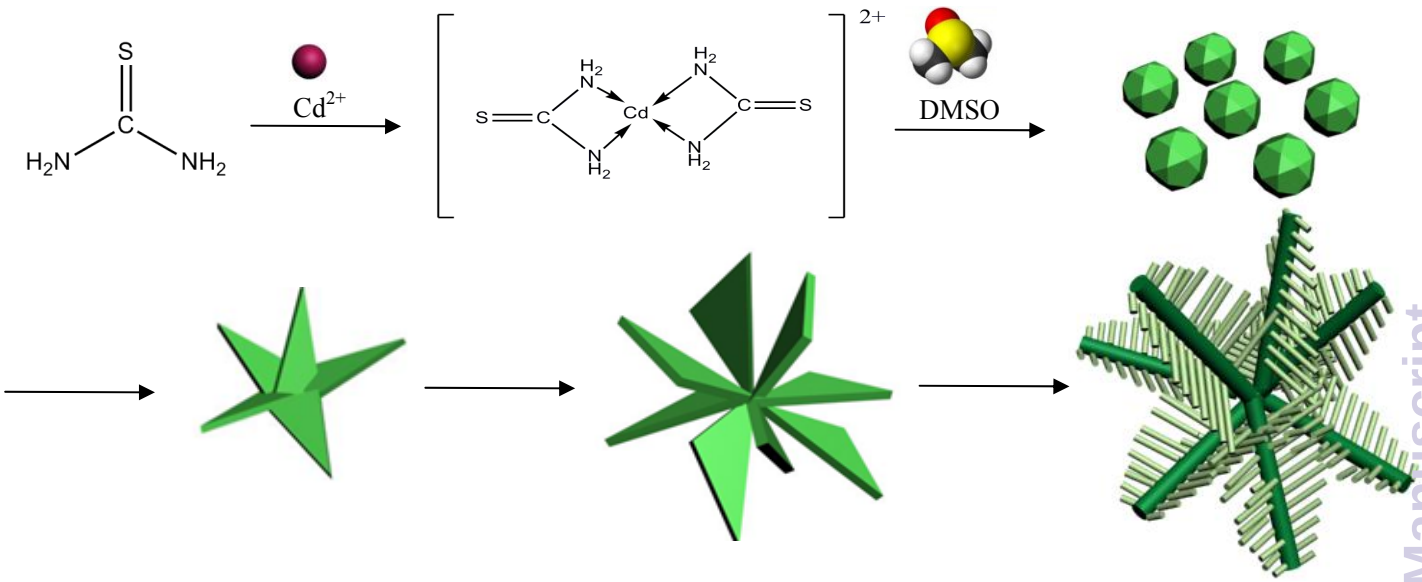

Fig. 4 Zhou Yu et al.

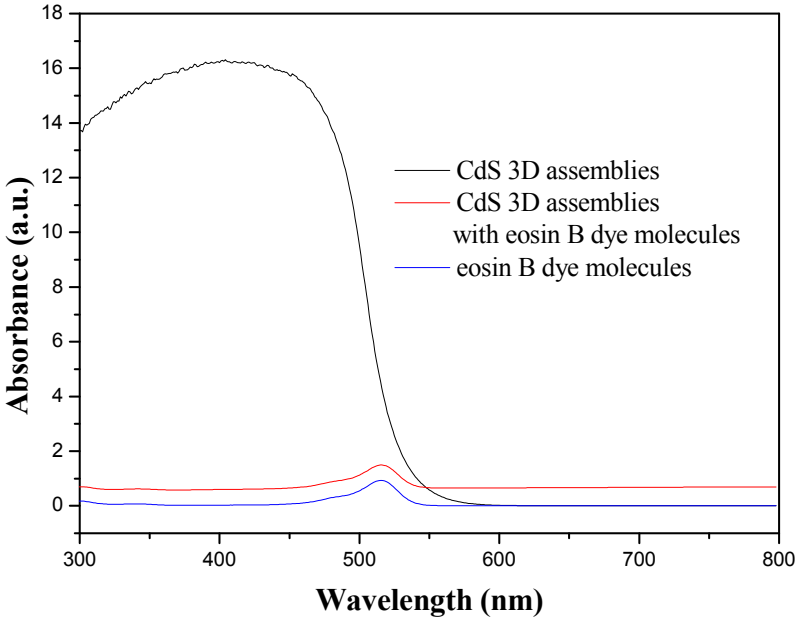

Fig. 5 Zhou Yu et al.

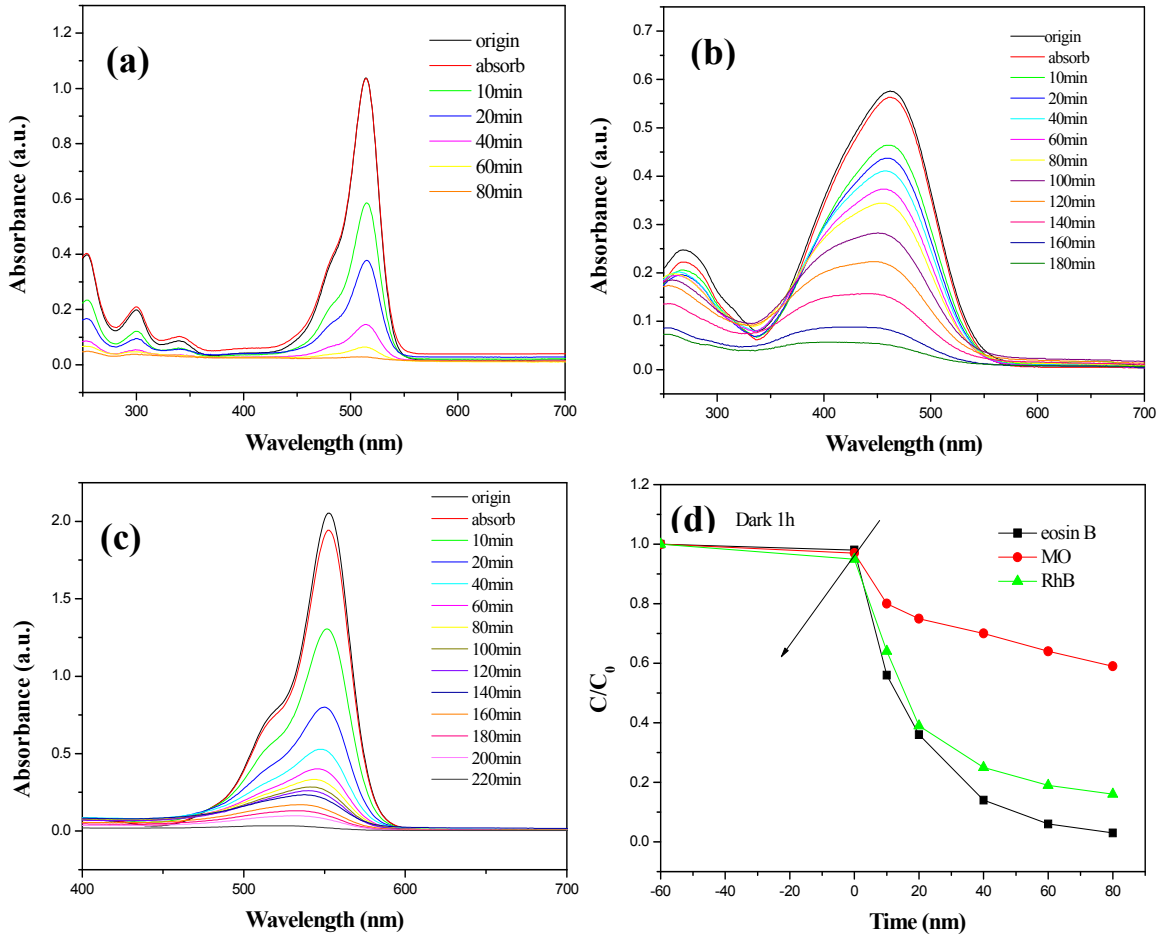

Fig. 6 Zhou Yu et al.

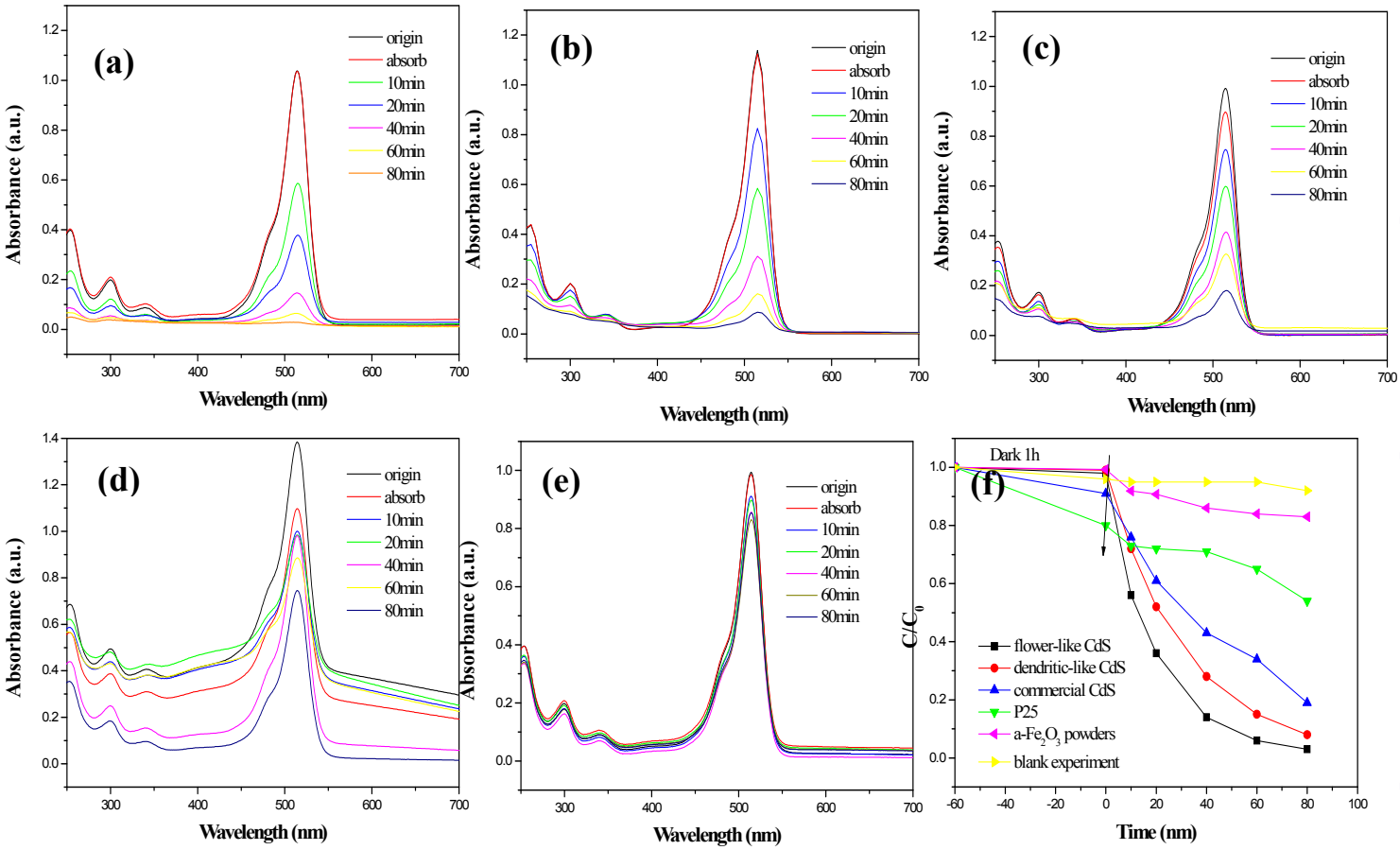

Fig. 7 Zhou Yu et al

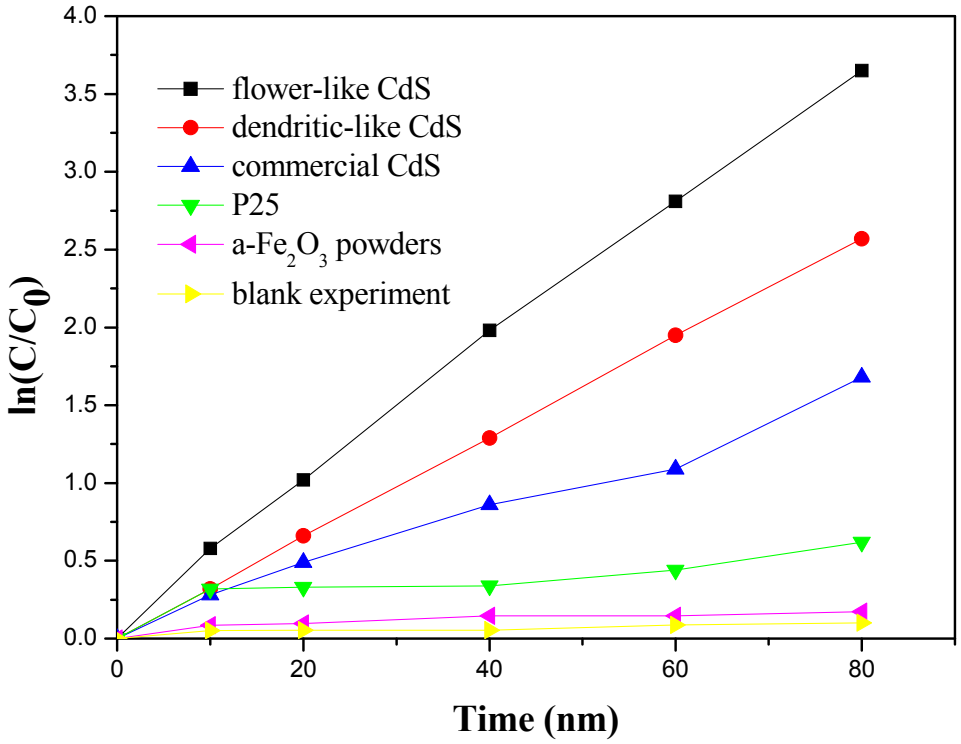

Fig. 8 Zhou Yu et al

Graphical Abstract

In this paper, novel CdS 3D assemblies are prepared via a facile and effective hydrothermal route using dimethyl sulfoxide as the growth template. A possible growth mechanism for CdS assemblies was proposed based on the experimental results. In addition, CdS assemblies exhibit superior photocatalytic activities by the photodegradation of eosin B, Methyl orange (MO) and Rhodamine B (RhB) under visible light irradiation, with a comparison with other CdS nanostructures, P25 and a-Fe_2O_3 powders, demonstrating potential applications in removal of organic dye molecules from waste water.